Fuel 381 (2025) 133441

Contents lists available at ScienceDirect

Fuel

journal homepage: www.elsevier.com/locate/fuel

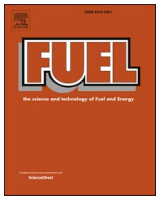

Full Length Article

Parametric investigation of diesel–methanol dual fuel marine engines with port and direct injection

Panagiotis Karvounis [a,*], Gerasimos Theotokatos [a], Chaitanya Patil [a], La Xiang [b], Yu Ding [b]

[a] Maritime Safety Research Centre, Department of Naval Architecture, Ocean, and Marine Engineering, University of Strathclyde, Glasgow G4 0LZ, United Kingdom
[b] College of Power and Energy Engineering, Harbin Engineering University, Harbin, China

ARTICLE INFO

Keywords:
Methanol combustion
Marine dual fuel engine
Direct injection
Port injection
CFD modelling

ABSTRACT

Methanol is identified as a transition fuel to improve the environmental footprint of shipping operations. However, high methanol shares cannot be achieved in premixed combustion marine dual-fuel engines. This study aims at parametrically investigating the impact of two types of methanol injection, namely port and direct injection, on marine engines by employing CFD modelling. A large medium speed marine engine with nominal power of 10.5 MW at 500 rev/m is considered. CFD models are developed for the engine diesel and dual fuel modes with methanol port or direct injections. Several cases with methanol energy fractions ranging up to 50 % for the port injection and 95 % for the direct injection cases are investigated. The developed CFD models were validated for the investigated engine operation in the diesel gas modes, as well as for a small engine with methanol port injection. A parametric study considering the engine settings and methanol energy fraction is performed to identify the engine settings and limits for the combustion knock-free operation for high methanol shares. Subsequently, the comparative assessment of the investigated marine engine performance and emissions parameters is performed for the considered cases. This study results reveal that the methanol direct injection can use up to 95 % methanol energy fraction retaining knock-free combustion conditions, whilst reducing NOx emissions by 85 %. The engine indicated thermal efficiency increases at higher methanol energy fractions for direct injection, whereas opposite trade-offs are exhibited for premixed combustion. Methanol use shortens the combustion durations compared to the diesel mode, reducing the maximum temperature by 1–3 %. This study provides valuable insights delineating the impact of the settings to the marine engines performance and emissions trade-offs, hence contributing to developing methanol fuelled marine engines.

1. Introduction

The shipping sector seeks to effectively address its decarbonisation. Following the Paris Agreement [1], the International Maritime Organisation (IMO) proposed measures, such as Emission Control Areas (ECAs) [2], Energy Efficiency Design Index [3], and Carbon Intensity Index, whereas net-zero CO_2 emissions are targeted by 2050 [4]. The use of alternative fuels in marine engines is a pathway to achieve these targets.

Methanol is perceived as a short-term solution in the shipping sector transition towards zero-carbon fuels [5]. Notably, methanol, a potentially renewable fuel [6], exhibits distinct characteristics compared to conventional diesel, which include its high molar expansion, leading to in-cylinder pressure increase, even in the absence of external heat addition. Methanol high octane number, low cetane number, and high laminar flame velocity, renders it unsuitable for compression ignition combustion within practical compression ratio ranges [7]. Karvounis et al. [8] reported that several factors exert significant influence on engine performance for dual-fuel operation. The methanol increased latent heat of vaporisation, relative to diesel, may have contradictory effects on the formation of nitrogen oxides (NOx) emissions and the engine overall brake thermal efficiency. Several studies [9–11] investigated both port and direct injection of methanol in heavy duty engines, revealing that the methanol use resulted in reduced maximum in-cylinder pressure due to the methanol high heat of vaporisation. Furthermore, the ignition delay prolongs for higher methanol energy fraction [12,13]. Conversely, there exists limited literature addressing the increase of methanol energy fraction in marine engines and the corresponding variations in engine performance parameters. Li et al. [14] investigated different combustion strategies for high methanol

Abbreviations: BL, Baseline Case; BTDC, Before Top Dead Centre; CFD, Computational Fluid Dynamics; DI, Direct Injection; ITE, Indicated Thermal Efficiency; MEF, Methanol Energy Fraction; PI, Port Injection; RI, Ringing Intensity; TDC, Top Dead Centre.

* Corresponding author.
E-mail address: panagiotis.karvounis@strath.ac.uk (P. Karvounis).

https://doi.org/10.1016/j.fuel.2024.133441
Received 11 July 2024; Received in revised form 23 September 2024; Accepted 13 October 2024
Available online 22 October 2024

Nomenclature

CA50	Crank Angle at which 50 % of the heat from combustion is released (^{o}CA)
CA90	Crank Angle at which 90 % of combustion is released (^{o}CA)
CO	Carbon Monoxide (ppm)
D_{eff}	Effective Diameter
HRR_{peak}	Peak Heat Release Rate (J/^{o}CA)
L_b	Breakup Length
P_{max}	Maximum in-cylinder Pressure (bar)
T_{max}	Maximum in-cylinder Temperature (K)
T_{mean}	Mean in-cylinder Temperature (K)
Y	Mass Fraction of Species
η_c	Combustion Efficiency (–)
ρ	Density (kg/m^3)
Φ	Equivalence Ratio (–)
Ω	Collision Integral

energy fractions, concluding that the compound-combustion approach leads to an increase in the maximum heat release rate (HRR) as methanol energy fraction rises. Premixed combustion is less efficient when compared to the direct injection method, which accommodates higher methanol energy fractions.

Li et al. [15] conducted a parametric investigation of the methanol direct injection in a diesel engine, revealing that smaller injector nozzle diameter results in higher injection pressure, consequently higher peak HRR and maximum cylinder pressure, whereas the nozzle spatial angle exhibited limited impact on HRR or emissions. Valentino et al. [16] investigated the performance of a high-speed diesel engine using n-butanol mixtures under premixed combustion conditions, concluding that meticulous control of injection timing, injection pressure, and oxygen concentration at intake enables efficient premixed combustion, leading to reduced smoke and NOx emissions.

The use of alcohol-based fuels, such as methanol and ethanol, in internal combustion engines primarily stemmed from their advantageous properties in mitigating knocking phenomena. However, recent investigations argued that the occurrence of knocking, and the onset of roar combustion impose limitations on the methanol energy fraction, which can reach 45 % for the premixed combustion engines [17]. Notably, Liu et al. [18] and Song et al. [19] proposed an upper boundary ranging from 70 % to 85 % for the methanol mass fraction at medium to high loads for the premixed combustion engines. The upper methanol energy fraction limit depends on factors including the compression ratio and the boost pressure, which they impact the susceptibility to knock. At higher loads, particularly in premixed combustion mode, the occurrence of roar combustion and, subsequently, knock phenomena represent the primary constraints on the maximum attainable methanol energy fraction. This limitation arises due to a higher degree of premixed mixture, combined with the higher compression ratio characteristic of diesel engines, which can potentially induce end-gas autoignition [20]. Dierickx et al. [21] concluded to a maximum methanol energy fraction ranging 30–38 % for a high-speed diesel engine operating at high loads.

Recently, the marine engine manufacturers introduced versions of methanol fuelled engines. The first marine two-stroke methanol engine with water injection to meet the IMO Tier III NOx emissions regulations is reported in [22]. The marine four stroke engine with methanol direct injection is reported in [23]. Marine engines operating with methanol port injection and premixed combustion are reported in [24]; these engines employ methanol energy fractions up to 50 %. However, the methanol energy fraction limit for these engines is affected by the operating point (load and speed), whereas high diesel fuel energy fractions are employed to assure knock-free combustion conditions. The literature does not provide guidelines on the preferred methanol injection methods (port or direct), the diesel substitution ratio, and limitations that must be addressed for new-built and retrofitted engines. Usually, methanol marine engines are expected to additionally operate at the diesel mode for redundancy purposes. The marine dual-fuel engines operating with methanol are still understudied in the pertinent literature.

Based on the preceding literature review, the following research gaps are identified: (a) lack of comprehensive investigations dealing with marine engines operating at high methanol energy fractions to identify trade-offs in engine performance and emissions parameters; (b) lack of understanding of methanol combustion strategies in marine engines and their suitability; (c) lack of marine engines investigations focusing on conditions leading to unstable combustion phenomena, defining envelopes for knock-free combustion conditions.

The aim of this study is to parametrically investigate the impact of two types of methanol injection, namely port and direct injection, on marine engines by employing CFD modelling. The limits in parameters, such as the methanol energy fraction, are identified for both injection types, whereas settings and conditions that facilitate the knock-free combustion and engine operation at the highest efficiency are determined.

The novelty of this study stems from: (a) comparative assessment of both methanol port and direct injection for a large marine four-stroke engine, revealing each method advantages and limitations; (b) derivation of trade-offs between performance parameters and emissions for varying MEFs; (c) the delves into the understanding of key limitations on methanol energy fraction utilisable under different combustion methods (port and direct injection). Such information is crucial for the engine optimisation meeting emissions regulations. This study provides insightful information to address challenges associated with the adoption of methanol-fuelled marine dual-fuel engines, hence supporting the maritime industry to achieve lower emissions footprint.

2. Methodology

Fig. 1 illustrates the methodological steps employed in this study. Step 1 focuses on the characteristics and settings of the considered marine engine. Step 2 deals with the development of a computational fluid dynamics (CFD) model for the diesel mode using the CONVERGE software. The engine injection parameters reported in the engine shop trails were employed to set up the injection sub-model. Step 3 includes the grid sensitivity study leading to the compromise between error and computational effort. Step 4 includes the validation of the CFD model results against available experimentally acquired parameters corresponding to the diesel and gas modes, as well as published measurements from a small methanol fuelled engine.

Steps 5a and 5b employed the validated CFD model as baseline to develop CFD models for the dual fuel operation with methanol (for both methanol direct injection and port injection) changing the reaction mechanism and fuel properties. For the direct injection, both methanol and diesel fuels are injected from the same injector nozzle considering different holes and injection angles.

Step 6 deals with the operating envelope identification and the parametric investigation to determine the temperature and pressure at the inlet valve closing as well as the exhaust gas recirculation ratios that facilitate knock-free combustion conditions and high combustion efficiency. Step 7 focuses on the comparative assessment for different methanol energy fractions. Step 8 includes the engine settings determination for each methanol energy fraction (MEF) and combustion method to ensure knock-free combustion conditions at high loads. Finally, a comparison between the premixed and diffusive combustion methods for different MEFs is performed to identify differences in the emissions and performance parameters trade-offs.

For ascertaining the knock-free combustion in methanol fuelled engines, the use of EGR is considered. The study focuses on a nine-cylinder, four-stroke marine engine, the particulars of which are listed in Table 1. Detailed description of the engine is provided in Stoumpos et al. [26].

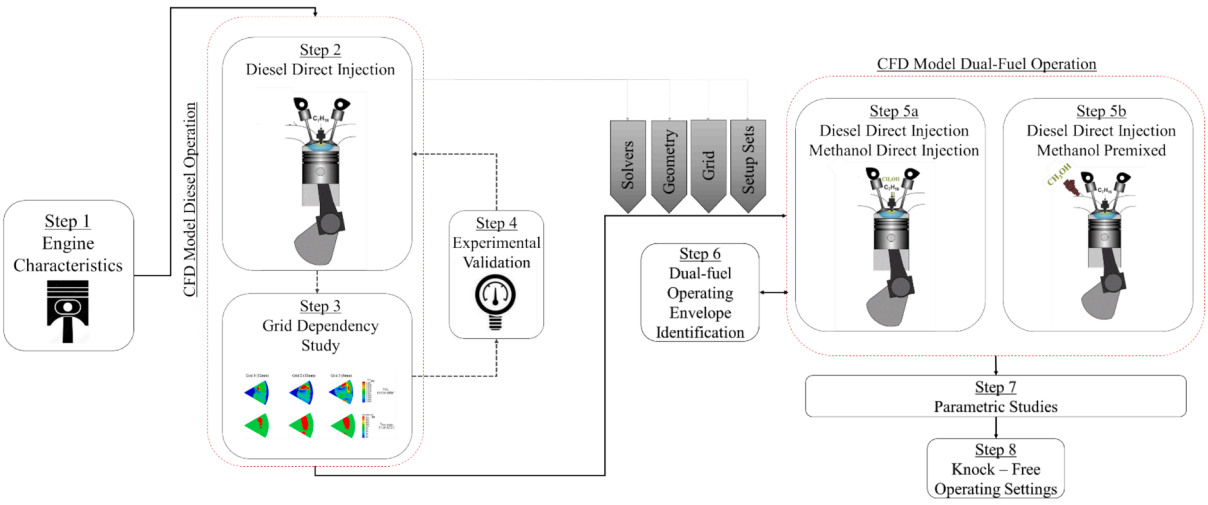

Fig. 1. Methodology flowchart.

This study considered the following assumptions. Ideal gas state was assumed to represent the in-cylinder working medium thermodynamic behaviour. The power output per cylinder was assumed the same for all the engine cylinders A reaction mechanism with 672 reactions and 143 species was selected, which can adequately represent diesel, and alcohol fuels according to [32]. The SAGE combustion model with the default values for its constants was employed for both the diesel and dual-fuel modes. A two-dimension adaptive zoning that conserves NOx during species remapping was used. A preconditioned, constant volume iterative solver was employed, with the relative tolerance equal to 0.0001, and the iteration error for each species equal to 10^{-14} [60]. Trapezoidal pressure pulses were considered for the direct injection of the diesel and methanol fuels [58]. The KH-RT spray break up model (considering the default values for its constants) was employed for the diesel and methanol direct injection. The RT model breakup time, model size and length constants were set to 1.0, 0.1, and 9.9 10^5, respectively. The KH model breakup time constant and model size constant was considered 7 and 0.61 respectively, according to Bravo and Kweon [60]. Exhaust gas recirculation (EGR) was considered as the knock mitigation measure, with the EGR ratio being dependant on the methanol energy fraction and injection method. For the premixed combustion mode, the initial in-cylinder air–fuel mixture was considered homogenous.

2.1. CFD model

The CFD model was set up by following the steps shown in Fig. 2. The engine cylinder geometric parameters were employed to determine the computational grid. To reduce computational effort, the symmetries of both the cylinder and the injector were considered, leading to the selection of a sector corresponding to one sixth of the engine cylinder. The employed sub-models are listed in Table 2. The in-cylinder pressure, temperature and composition are governed by the conservation equations including mass, momentum, and energy transport. The boundary and initial conditions of the CFD model for the diesel mode are presented in Table 3.

Table 1
Marine engine characteristics.

Parameter	Value
Type	Wärtsilä 9L46C
Brake Power at MCR point (kW)	10,500
Speed at MCR point (r/min)	500
Cylinders Number (–)	9
Compression Ratio	14.0:1
Bore/Stroke (mm)	460 / 580
Diesel Start of Injection (°CA BTDC)	6
Diesel Injection Pressure (bar)	1,000
Nozzle angle (deg)	67.5
Spray Cone Angle (deg)	17.5
Nozzle Diameter (mm)	0.78
Nozzle Holes Number (–)	6
Simulated cycle period	IVC – EVO 135°CA BTDC–135°CA ATDC

MCR: maximum continuous rating.

The ringing intensity (RI) is employed to represent in-cylinder excessive oscillations (knocking) and the knocking onset for a wide range of engine operating conditions [36]. The RI upper limit for four-stroke medium speed marine engines ranges 4–5 MW/m^2; beyond this limit, roar combustion intensifies leading to knocking conditions [37]. RI (in MW/m^2) is calculated according to the following equation:

$$RI = \frac{1}{2\gamma}\frac{\beta\left(\frac{dp_{max}}{d\theta}\right)_{max}}{p_{max}}\sqrt{\gamma R T_{max}} \tag{1}$$

where $\left(\frac{dp_{max}}{d\theta}\right)$ denotes the rate of in-cylinder pressure; γ is the ratio of the specific heats; R is the gas constant; T_{max} is the maximum mass-averaged in-cylinder temperature; β denotes the tuning parameter that relates the amplitude of pressure pulsations with the maximum pressure rise rate and is considered 0.05 herein [25]. The operational limitation in this study comes from RI and is set to 4 MW/m^2 according to literature.

The injection pressure is determined based on the injector geometry and the injected fuel mass (which is provided as input), as well as the fuel physical properties, based on the following equation [56]:

$$p_{inj} = \frac{\rho_f\left(\frac{m_f}{C_D\rho_f A_{nozzle} f_g}\right)^2 + 2p_{cyl,b}}{2} \tag{2}$$

where ρ_f is the fuel density, C_D is the discharge coefficient, A_{nozzle} is the geometric area of the injector nozzle, f_g is the geometrical characteristics factor equals to $\frac{n_{holes}}{n_{nozzle}}$. Since this is a factor related to the injector number of holes and number of nozzles it can be used either for single-hole or multi-hole nozzles regardless of the configuration. p_{cyl} is the in-cylinder back pressure and m_f denotes the fuel mass flow rate. Typically, the injection pressure is input in the spray breakup model. However, CONVERGE employs as input the fuel mass flowrate, the injector characteristics and discharge coefficient to calculate the injection pressure, which is subsequently used in the spray model.

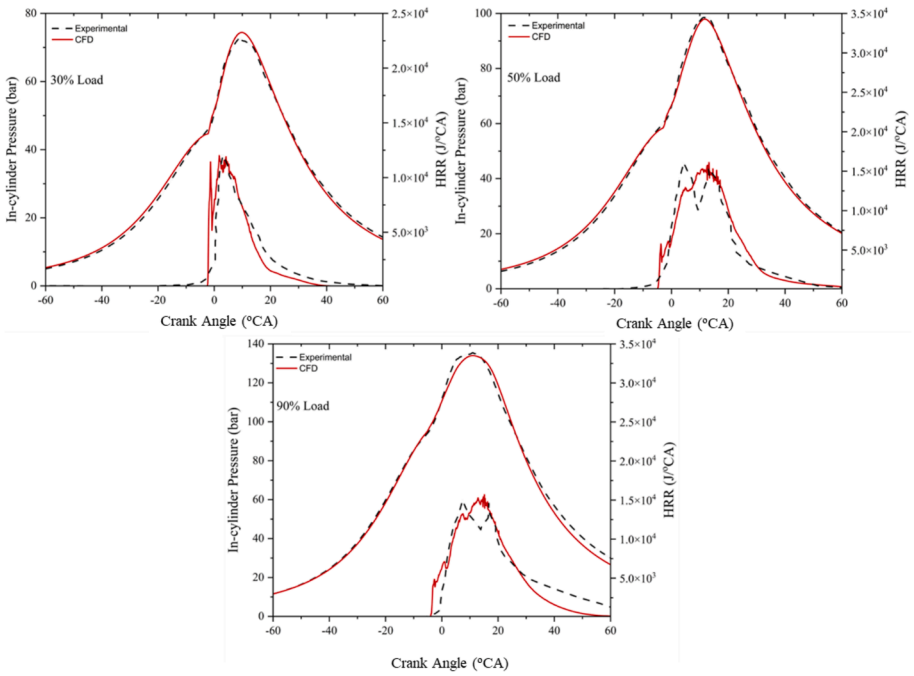

Fig. 2. Simulated and measured in-cylinder pressure and heat release rate for the investigated marine engine operating in the diesel mode for 30%, 50% and 90% loads.

Table 2
Employed models and mechanisms for the developed marine engine CFD model for the diesel and dual fuel (DF) modes with port injection (PI) and direct injection (DI).

Mechanism/model	Diesel Mode	DF Methanol PI	DF Methanol DI	Comment
Reaction Mechanism	Semi-detailed chemical kinetic model consisting of 142 species and 672 reactions reported in Andrae and Head [33]			
Combustion model	SAGE: Two adaptive zones; Solving analytical Jacobian matrix; Absolute tolerance: 10^{-14}			Detailed chemical kinetics solver. Calculates the reaction rates for each elementary reaction.
NOx Mechanism	Extended Zeldovich [31]: Thermal NOx model; Mass scaling factor to convert NO to NOx: 1.533			
Turbulence Model	RANS k-ε			Provides lower accuracy compared to LES, however extensively used in combustion modelling due to its acceptable accuracy and low computational cost [62]
Droplet breakup model	KH-RT; size constant: 0.61; velocity constant: 0.188 [27]			The Kelvin-Helmholtz instability is based on a liquid jet stability analysis.
	Mass diffusivity constants			The mass diffusivity constants pertain to the fuels that are injected directly in-cylinder. These constants are experimentally determined. The liquid spray breakup model is described in reference [63].
	C_7H_{16} D_0 = $5.9410^{-6}n_0$ = 1.6	C_7H_{16} D_0 = $5.9410^{-6}n_0$ = 1.6	C_7H_{16} D_0 = $5.9410^{-6}n_0$ = $1.6CH_3OH$ D_0 = $7.910^{-6}n_0$ = 1.87	
Droplets collision model	Negative Temperature Coefficient [29]			The method uses Monte Carlo calculations and exhibits higher accuracy compared to alternatives (O'Rouke model) whereas the computational cost is a linear of the parcels number.
Wall heat transfer	Han & Reitz [30]			The Han and Reitz model is employed.
Spray/Wall interaction model	Han [28]			Represents spraywall impingement processes that take place in internalcombustion engines.

$$MEF = \frac{m_{CH_3OH} LHV_{CH_3OH}}{(m_D LHV_D) + (m_{CH_3OH} LHV_{CH_3OH})} \quad (3)$$

The diesel fuel substitution with methanol is considered based on the energy fraction. The methanol energy fraction (MEF) is calculated according to the following equation [56].

where m and LHV denote the mass and the lower heating value of fuel, respectively.

The EGR ratio is defined according to the following equation is employed to define the in-cylinder initial conditions:

$$EGR = \frac{m_{EG}}{m_{EG} + m_{air}} \quad (4)$$

2.2. Grid sensitivity studies and experimental validation

Grid sensitivity study is discussed in Appendix A. According to Table 4, the simulation results for Grid-3 and Grid-4 exhibit small differences in terms of error on maximum pressure and RMSE on in-cylinder pressure. The results indicate that Grid 3 is an effective compromise considering computational effort and accuracy. The average NOx emissions at exhaust valve opening (EVO) almost remain constant for the three grids; however, their spatial in-cylinder distribution varies. As shown in Fig. A1a, Grid–3 leads to the convergence of the derived results the in-cylinder temperature and NOx emissions, as smaller variations compared to the respective Grid–2 results are exhibited. For the cases that considered methanol combustion (either

Table 3
CFD model boundary and initial conditions for the investigated marine engine diesel mode.

Boundary Conditions	Value	Comment
Cylinder head Temperature (K)	530	Values calculated from 1D thermodynamic model developed by Tsitsilonis et al. [34], corresponding to warmed up conditions.
Cylinder liner Temperature (K)	430	
Piston Temperature (K)	550	
Initial Conditions		
Temperature at the IVC (K)	360	Calculated from turbocharger isentropic expansion ratio under the assumption of ideal gas law and considering the boost temperature and pressure from the shop trials.
Pressure at the IVC (bar)	2.8	
Turbulent kinetic energy (m^2/s^2)	62.02	Default values were used. A parametric investigation was conducted to determine these parameters influence on the results.
Turbulent dissipation (m^2/s^3)	17,183	
Liquid diesel spray temperature at the time of injection (K)	340	Within the range of experimental results reported in Siebers [35].

Table 4
Computational grids characteristics.

Parameter	Grid 1	Grid 2	Grid 3	Grid 4
Element size (mm)	12	10	8	6
Maximum Number of Cells*	10,900	18,838	36,800	87,216
Error on p_{max} (%)	5.2	2.4	2.3	2.3
RMSE on in-cylinder pressure (bar)	4.96	4.93	4.91	4.90
Adaptive mesh refinement	On between 12 °CA BTDC and 135 °CA ATDC			
Velocity Max Embedding Level	3	3	4	4
Temperature Max Embedding Level	3	3	4	4
Number of Cores Used	40 Intel Cores IPM			
Simulation run duration (h)	3	4.5	9.5	23

*At TDC not including embedding and mesh refining.

port or direct injection), the results with Grid–3 demonstrated satisfactory convergence.

The CFD model validation is conducted using the in-cylinder pressure acquired during shipboard measurements, which was first corrected to remove offsets [34], and then employed to calculate the heat release rate. Table 5 lists the error between the CFD model results and respective measured parameters, considering the maximum in-cylinder pressure, the power output, and NOx for three loads corresponding to engine healthy operating conditions as retrieved from shop-test trials of the manufacturer. For 50 %, 75 % and 100 % loads, the predicted power output exhibited deviations of 4 %, 3.4 %, and 1 % (compared to the measured values), the peak in-cylinder pressure exhibited errors of 0.3 %, 2.6 %, and 0.5 %, whereas the NO emissions errors were found 8.9 %, 8 % and 3.3 %, respectively.

Fig. 2 showcases the predicted and measured in-cylinder pressure and heat release rate for 30 %, 50 % and 90 % loads. Median-averaging was applied to reduce noise for the experimental data. The CFD results are in satisfactory agreement with the experimental data, both in terms of in-cylinder pressure and heat release rate at all examined loads. Deviations from the measured values are attributed to engine fouling and overall degradation, arguments that are supported by previous studies [38,39]. Additionally, CFD sub models epistemic uncertainty and calibration also impact the results accuracy. The engine measurements were not performed under ideal test-bench conditions, leading to errors. It must be noted though the lack of emissions measurements to calibrate the emission sub-model. Additionally, according to ISO 15550:2002 shop test trials are conducted with 5 % error.

In the absence of experimental data for methanol-fuelled marine engines, and to test the CFD model with a more complex combustion process involving two fuels, the closed cycle of the investigated marine engine is modelled considering the gas mode operation with premixed natural gas and direct pilot diesel injection. The same reaction mechanism and computational mesh remains are employed for all modes (diesel, gas and methanol). Natural gas is injected in the port manifold and pilot diesel is directly injected in-cylinder to initiate the reactivity-controlled combustion of the premixed air–natural gas mixture. The derived simulations results and comparisons with corresponding measured parameters from the engine shop tests are presented in Appendix E. The estimated errors for the in-cylinder maximum pressure and NOx emissions predictions were found below 8 %, whereas consistent trends with the errors estimated for the diesel mode are observed. This demonstrates the employed CFD model capability to represent the more complex in-cylinder processes for the engine gas mode (compared to the diesel mode).

In addition, the developed CFD model was validated using reported experimental data for a small-scale high-speed diesel engine operating in the dual fuel mode employing methanol port injection with 30 % MEF at 75 % load. Details of the engine and experimental procedure are provided in Zang et al. [57]. The simulated and experimentally derived variations of the in-cylinder pressure and heat release rate as well as NOx and Soot emissions are presented in Fig. 3. NOx and Soot emissions present errors below 7 % which is within computational model acceptance rate. The error on the in-cylinder maximum pressure was found 0.5 %, whereas the crank angle at the maximum pressure was predicted at 9.1 °CA ATDC instead of the measured 7.5 °CA ATDC. The RMSE for the in-cylinder pressure was found 6 bar, which is comparable to the respective RMSE values estimated for the diesel mode for the marine engine. The simulated heat release rate demonstrates a higher value of the premixed combustion peak compared to the experimental data. However, the simulation results are in alignment with the trade-offs presented in Zang et al. [57], where their CFD model slightly overestimated the premixed part of combustion. Therefore, it is inferred that the developed CFD model provides adequate accuracy for the methanol-fuelled small-bore engine operating in dual fuel mode.

Based on the preceding discussion and the presented validation cases, it is deduced that the developed CFD model (and its versions for the investigated diesel and dual fuel modes with port (premixed) and direct methanol injection) can be employed with the highest possible confidence for the simulation of the considered methanol cases at various MEF and injection methods in this study.

2.3. Cases description

The considered test cases with varying MEFs primarily focused on conditions at medium to high engine loads. This is due to the occurrence of knocking phenomena, which becomes particularly pronounced in these loads, thus imposing significant constraints for the practicable

Table 5
Simulated and measured (shop tests) maximum in-cylinder pressure, power output and NO emissions for the considered marine engine operation in the diesel mode.

Load (%)	Maximum Pressure			Indicated Power Output			NO emissions		
	Measured (bar)	*CFD (bar)*	*Error (%)*	*Measured (kW)*	*CFD (kW)*	*Error (%)*	*Measured (ppm)*	*CFD (ppm)*	*Error (%)*
50	135	135.4	0.3	4725	4900	4.6	9679	10,500	8.9
70	156	160	2.6	7088	6850	3.4	9296	10,100	8.0
100	205	204	0.5	9450	9440	1.0	9179	9390	3.3

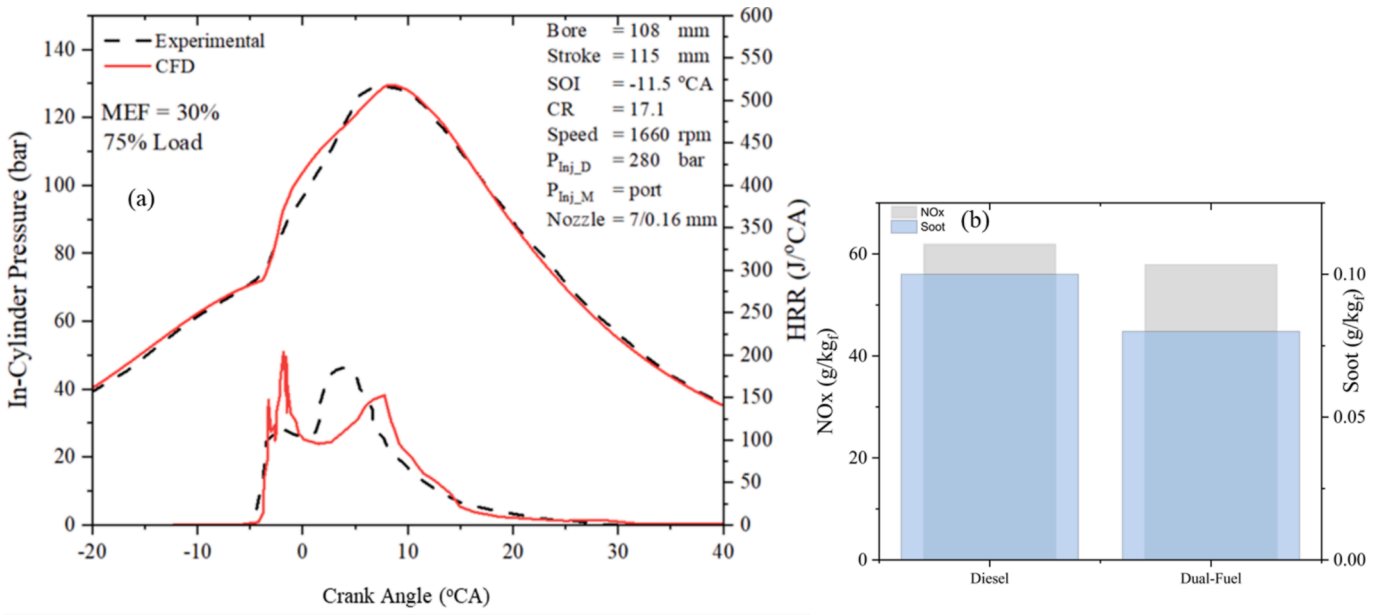

Fig. 3. Simulated and measured (from [57]) a) in-cylinder pressure and heat release rate and b) NOx and Soot emissions for a high-speed light duty engine operating in the dual fuel mode (diesel-methanol) with methanol port injection (30% MEF) at 75% load.

methanol use, as supported by the findings in Wang et al. [17]. Table 6 presents the considered cases particulars listing the fuel injection timings, in-cylinder pressure and temperature at the intake valve closing (IVC), and EGR ratios. These parameters are investigated to identify settings leading to combustion without knocking or ringing, and acceptable combustion efficiency.

For the baseline (BL) case corresponding to the diesel mode, the initial conditions were derived considering the engine shop trials, whereas the 30 % EGR rate is used for benchmarking purposes with the other cases. For premixed methanol combustion cases, 50 % MEF was assumed to be the upper limit [40,41] to effectively avoid extensive knocking, whereas EGR is employed to supress knocking. The EGR ratio values are selected according to Senecal et al. [42], with the highest value being 30 %. For 80 % MEF, several EGR values are tested. The diesel injection timing and pressure were considered constant for the investigated methanol premixed combustion cases.

Each case achieves the same power output with the diesel mode by adjusting the mass of fuels injected. Additionally, the injection parameters and initial conditions are modified to obtain knock-free combustion conditions for the considered MEF for the examined injection methods.

For the premixed combustion cases, a 30 % EGR ratio is found to be essential in reducing in-cylinder reactivity and thereby preventing extensive knocking and ringing. For the 8M2D-PI case, several techniques were explored to mitigate the rapid pressure increase rate, including high EGR rate (up to 45 %) [14], increased temperature at IVC [43], and reduction of charging pressure (the latter can be achieved by using waste gate valve [44]). However, these measures did not effectively mitigate extensive ringing. Therefore, 50 % MEF was taken as the upper limit for methanol premixed combustion cases.

The methanol direct injection cases accommodated MEFs up to 95 % without significant modifications to the injection timings and initial conditions. For cases involving MEFs higher than 50 %, moderate EGR (up to 15 %) is used. The temperature at IVC gradually increases from 360 K to 380 K for the 80 % MEF case, and to 400 K for the 90 % and 95 % MEF cases. This enhances the in-cylinder reactivity, as the methanol high latent heat of vaporisation cools the in-cylinder mixture inhibiting combustion [45]. MEF increase leads to the ignition delay increase [46], necessitating a slight retardation of the pilot injection timing in these cases (from 6°CA ATDC to 7°CA ATDC).

3. Results

This section presents the results and their corresponding analysis. Sections 3.1, 3.2 and 3.3 present and discuss the derived trade-offs in the in-cylinder parameters, emissions, and engine parameters respectively, for the two methanol injection methods and the considered MEF. This section presents the results and their corresponding analysis.

Table 6
Particulars of the investigated cases with methanol port (PI) and direct injection (DI).

Methanol Injection Method	Case Study Code	MEF (%)	Diesel Injection	Methanol Injection	In-cylinder Pressure at IVC* (bar)	In-cylinder Temperature at IVC (K)	EGR ratio (mass %)
	BL	0	6°CA BTDC*	–	2.8	360	30
Port Injection	1M9D-PI	10	6°CA BTDC	Port	2.8	360	30
	2M8D-PI	20	6°CA BTDC	Port	2.8	360	30
	5M5D-PI	50	6°CA BTDC	Port	2.8	360	30
	6M4D-PI	80	6°CA BTDC	Port	2.8	360	30
	8M2D-PI	80	6°CA BTDC	Port	2–2.8	340–400	10–45
Direct Injection	1M9D-DI	10	6°CA BTDC	25°CA BTDC	2.8	360	0
	2M8D-DI	20	6°CA BTDC	25°CA BTDC	2.8	360	0
	5M5D-DI	50	6°CA BTDC	25°CA BTDC	2.8	360	5
	8M2D-DI	80	7°CA BTDC	35°CA BTDC	2.8	380	13
	9M1D-DI	90	7°CA BTDC	44°CA BTDC	2.8	400	13
	9.5 M0.5D-DI	95	7°CA BTDC	44°CA BTDC	2.8	400	15

*IVC: Intake Valve Closing; BTDC: Before Top Dead Centre, ratio.

3.1. Effects on in-cylinder parameters

Fig. 4 presents the derived mean in-cylinder pressure variations for the investigated cases at 90 % load. For the port injection (PI) –premixed combustion– cases, the peak in-cylinder pressure varies from 125 bar for the BL case (diesel mode) to 127.5 bar, 135.7 bar, and 162 bar for MEFs of 10 %, 20 %, and 50 %, respectively. This is attributed to the higher methanol oxygen content, which renders the combustion faster. It is worth noting that a more rapid pressure increase (dp/dCA) is observed in the 5M5D-PI case, where methanol begins to dominate as the primary fuel. The rate of pressure increase is associated with the potential knocking occurrence, which is further discussed below. For premixed combustion cases with high MEF, the increased in-cylinder pressure leads to extensively unstable combustion.

For the direct injection (DI) cases, higher MEFs (up to 95 %) can be accommodated without significant unstable effects as methanol exhibits a shorter in-cylinder residence time. The peak in-cylinder pressure was found at 133 bar, 138 bar, 163 bar, 193 bar, and 190 bar for MEFs of 10 %, 20 %, 50 %, 80 % and 90 % respectively, compared to 125 bar pressure for the BL case. For 95 % MEF, the peak in-cylinder pressure reaches 170 bar, which is lower compared to the other MEF cases. This is due to the use of higher EGR to achieve knock-free combustion. Notably, 5 % diesel energy fraction can initiate the combustion process at high loads allowing the use of high MEF in dual fuel engines. It is also evident that a reduction in the compression work (compared to the BL case) is exhibited with increasing MEF. This is attributed to the higher methanol heat of vaporisation, as also supported by [47,48]. Fig. C1 (Appendix C) illustrates the reduction of compression work by considering the respective in-cylinder pressure variations.

Benchmarking the two injection methods, direct injection (DI) exhibits higher peak pressure for the same MEF (Fig. 4c, d), whereas the rate of pressure rise is higher in DI resulting in faster combustion.

Fig. 5 illustrates the heat release rate (HRR) variations for the considered cases for the PI and DI methods, as well as the BL case (diesel mode). Table 7 provides the CA at 50 % cumulative heat release (CA50) and 90 % cumulative heat release (CA90) along with the maximum relative pressure rate increase. The results for each case are compared to the diesel mode (BL) to highlight the main differences and provide trade-offs for marine engines.

As the MEF increases, the combustion shortens and the HRR rate is higher leading to higher peak HRR for both PI and DI.

For PI cases, as MEF increase the peak HRR increases from 16 kJ/^{o}CA in the BL case to 51 kJ/^{o}CA for 50 % MEF, while the greatest part of the combustion occurs closer to TDC as CA50 shifts to 7.6°CA ATDC from 14.6°CA ATDC. The first HRR peak is attributed to the premixed combustion of the diesel fuel prepared between diesel start of injection (SOI) and start of combustion (SOC) along with the methanol SOC.

For DI cases with low MEF, the combustion duration gradually reduces and the peak HRR advances, varying from 16 kJ/^{o}CA in the BL case to 16.7 kJ/^{o}CA and 18.1 kJ/^{o}CA for 10 % and 20 % MEF, respectively. Cases 8M2D-DI, 9M1D-DI and 9.5 M0.5D-DI require higher temperature at IVC to facilitate the methanol ignition, leading to higher peak heat release rates and significantly shorter combustion durations. The latter is also attributed to the higher methanol oxygen content (mixture with higher oxygen content) and richer mixtures considered. Case 9.5 M0.5D-DI (95 % MEF) yields lower peak HRR pertinent to 80 % and 90 % MEF due to the employed higher EGR ratio, and hence the reduced in-cylinder reactivity. It also exhibits larger ignition delay due to the reduced methanol cetane number compared to diesel that leads to poor ignitability. In addition, the time interval between CA50 and CA90 is 2.6°CA denoting a significantly shorter combustion duration. This brings the combustion start closer to 8°CA ATDC, leading to higher thermal efficiency [49]. For the 5M5D-PI case, the first peak at the HRR is attributed to the premixed methanol combustion along with a small amount of diesel prepared between the diesel SOI and start of combustion. The second peak is attributed to the diesel diffusive combustion and the remaining part of premixed methanol combustion. The second peak appears at 6.5°CA ATDC, which is close to the end of diesel injection. For the 5M5D-DI case, the first peak is attributed to diesel and methanol fuels that are mixed with intake air from their respective start

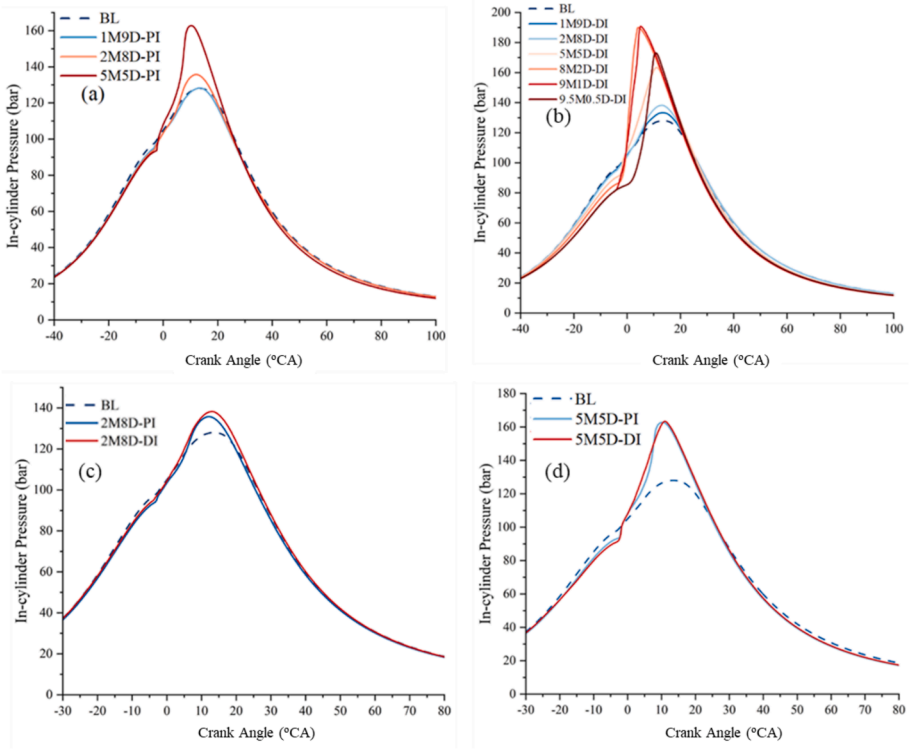

Fig. 4. In-cylinder pressure diagrams for the investigated cases at 90% load: (a) Port injection (PI), (b) Direct injection (DI), (c) port and direct injection with 20% MEF, and; (d) port and direct injection with 50% MEF.

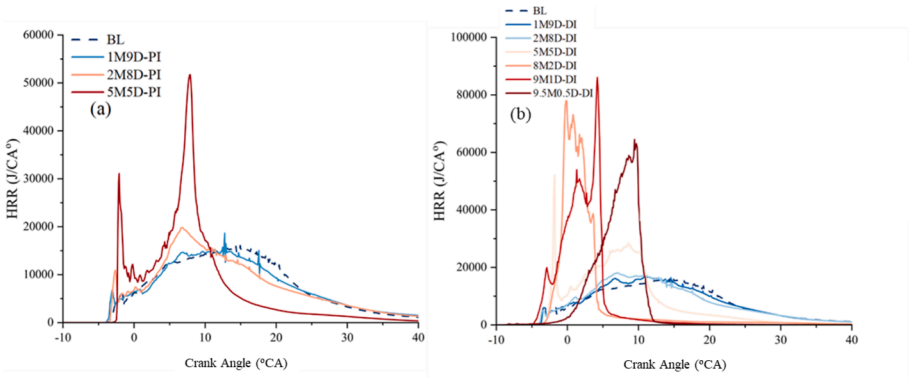

Fig. 5. Heat release rate diagrams for the investigate cases: (a) port injection (PI), (b) direct injection (DI).

Table 7
Rate of pressure increase, CA50 and CA90 for the examined cases.

Case	$(dp/d\theta)_{max}$ (bar/°CA)	CA50 (°CA)	CA90 (°CA)
BL	0.55	14.6	30.8
1M9D-PI	5.45	14	31.3
2M8D-PI	9.04	11.8	30.6
5M5D-PI	19.19	7.6	18.1
1M9D-DI	6.37	12.7	27.7
2M8D-DI	7.69	11.7	27.7
5M5D-DI	18.93	7.2	17.4
8M2D-DI	33.75	1	6.2
9M1D-DI	39.17	2.1	4.7
9.5 M0.5D-DI	36.75	7.5	10.1

of injection (6°CA BTDC and 25°CA BTDC for diesel and methanol). The second peak represents the diffusive combustion of both diesel and methanol fuels and is happening at 9°CA ATDC where the direct injection of both fuels is concluded.

In both cases (PI and DI), and due to the higher laminar flame velocity and methanol oxygen content compared to diesel, the combustion duration shortens, while methanol is consumed rapidly with CA50 and CA90 shifting from 14.6°CA ATDC and 30.8°CA ATDC for the BL case, to 11.8°CA ATDC and 30.6°CA ATDC for 2M8D-PI case, and to 11.7°CA ATDC and 27.7°CA ATDC for the 2M8D-DI case. For the port injection cases, the higher initial combustion rates are justified by the fact that more methanol is premixed with air prior to entering the combustion chamber. The increased heat release rate is also the limiting factor on higher than 50 % MEF uptake for the PI cases. For the DI cases, the ignition delay (as plotted in Fig. 6b) increases with the increase of MEF. The only change is at 95 % MEF that ignition delay is reduced slightly due to high EGR values applied to mitigate knocking tendency as heat release rate increases significantly with MEF.

Comparing the PI and DI cases, the former exhibits higher peak-HRR due to homogenous mixture and higher reactivity. Based on the preceding analysis, higher MEF results in shorter combustion duration and higher peak heat release rate compared to BL. PI cases exhibit longer combustion duration and higher peak heat release rates compared to DI.

Fig. 6a presents the ringing intensity (RI) as a function of methanol energy fraction (MEF). RI is associated with the maximum rate of in-cylinder pressure rise, which serves as an indicator of knocking intensity. It is inferred that the methanol use leads to increased knocking intensity, primarily due to its oxygen-rich nature compared to diesel, and the subsequent increased reactivity of the in-cylinder mixture. The in-cylinder reactivity can be assessed by the oxygen concentration along with temperature and pressure. Results presented in Fig. D1 (Appendix D) indicate higher reactivity for DI with 50 % MEF compared to PI, resulting in the HRR peak increase. Additionally, the richness of the mixture contributes to the knocking tendency at high loads and high MEFs. However, it is noteworthy that PI cases exhibit higher RI values compared to direct injection cases. This can be attributed to the longer in-cylinder residence

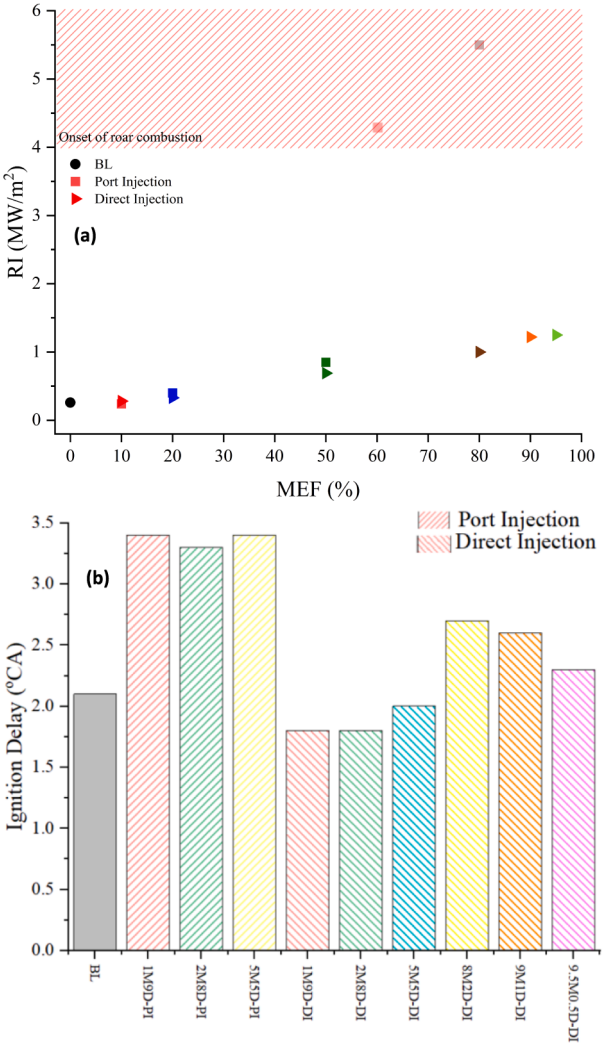

Fig. 6. Ringing intensity (RI) versus methanol energy fraction (MEF) (a) and ignition delay for the considered cases (b).

time (for PI case), in contrast to the relatively shorter residence time for the DI cases. For the former, the homogenous mixture and the methanol high laminar flame speed result in a rapid combustion. Compared to the baseline (BL) case, the RI exhibits an increase of 63 % for the 5M5D-PI case and 79 % for the 9.5 M0.5D-DI case. MEF increase beyond 50 % for the PI cases results in RI values greater than 4 MW/m^2. These findings support that the 50 % MEF is the upper limit for marine premixed combustion engines. Similar findings were reported in [50]. The preceding

analysis denotes that the higher MEF leads to higher RI, and hence engine operation in knocking conditions. The difference in RI compared with BL case, between the PI and DA cases becomes larger at high MEF. Increasing the methanol fraction in the dual fuel engine shifts the combustion towards TDC which is deemed causing increased the thermal stress. However, the latter is affected by the temperature increase in-cylinder along with the properties of piston material. In the dual fuel case, the maximum temperature rise for both port and direct injection is lower than in the diesel case. RI is highly influenced by the $dp_{max}/d\theta$ term that is significantly increased on dual fuel cases due to higher burning rate of methanol fuel pertinent to diesel one.

Fig. 6b demonstrates the ignition delay for the examined cases. For port injection cases as the mixture of methanol and air in the combustion chamber is deemed homogeneous, increased ignition delay is presented compared to the stratified charge formed when both fuels are directly injected in-cylinder. For high MEFs at DI cases the ignition delay is increased due to richer mixtures utilised in-cylinder. Also, as the MEF increases, the higher the reactivity requirements in-cylinder to achieve the start of combustion, hence ignition is shifted closer to TDC.

3.2. Effects on emissions

Fig. 7 illustrates the mass-based NOx concentration in the exhaust gas for the examined cases. The behaviour of NOx emissions in the presence of alcohol fuels, specifically methanol, exhibits contradictory trade-offs. The methanol high latent heat of vaporisation results in reduced in-cylinder temperature, while the higher oxygen content leads to faster burning rates promoting in-cylinder temperature increase [59]. The latter is true for methanol fuel, as more oxygen is available for the combustion process and therefore more energy per unit of fuel is produced yielding higher in-cylinder temperatures. Furthermore, the engine in-cylinder temperature and pressure at IVC affect the NOx emissions. For the PI cases, the NOx concentration decreases by 22 %, 25.4 %, and 30.5 % for MEFs of 10 %, 20 %, and 50 %, respectively. For the DI cases, NOx emissions increase by 7 % for the 1M9D-DI case, while they decrease by 1.2 %, 8.5 %, 71 %, 50 %, and 85 % for MEFs of 20 %, 50 %, 80 %, 90 %, and 95 %, respectively.

For MEF up to 50 %, PI cases exhibit a more pronounced reduction in NOx compared to the DI cases. Previous studies [51] demonstrated the influence of factors such as fuel stratification and cylinder reactivity on NOx formation. Since methanol direct injection results in higher fuel stratification, the NOx concentration is also higher for the DI cases, compared to the PI cases. Overall, the significant reduction in NOx emissions is attributed to the methanol evaporation cooling effect, which results in quenching the in-cylinder mixture and reducing its temperature.

The oxidation of CO to CO_2 is an indication of the combustion efficiency. The DI cases exhibit lower CO emissions compared to PI cases due to their less effective methanol fuel mixing. For DI cases, CO emissions increase with MEF, indicating lower combustion efficiency. 1M9D-DI and 2M8D-DI cases present lower CO than the respective PI ones, however, CO emissions increase from 1M9D-DI to 5M5D-DI. This can be attributed to the fact that combustion duration increases deteriorating the fuel utilisation for 1M9D-DI and 2M8D-DI. For 5M5D-DI the 5 % EGR used penalises the combustion efficiency and hence slightly increased CO concentration is observed. Nonetheless, for higher MEF the effect is counteracted by the increased charging temperature that increases in-cylinder reactivity promoting fuel utilisation. For the PI cases, the combination of high EGR values and leaner mixtures results in reduction of combustion efficiency and hence higher CO concentration is overall observed pertinent to the DI cases. The derived CO concentration results reveal that the combustion efficiency improves with the MEF, compared to the baseline (BL) case. In the 5M5D-DI case, complete combustion occurs, resulting in the complete conversion of CO to CO_2. Overall, the CO concentration varies from 0.82 g/kWh to 0.001 g/kWh from the BL to 95

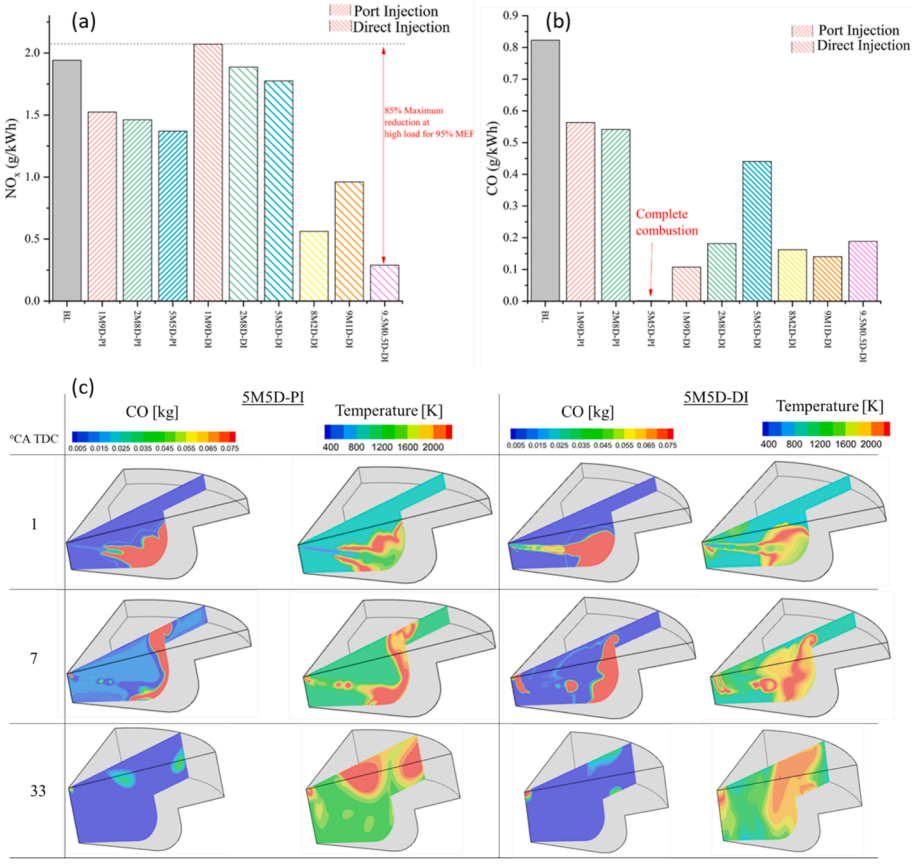

Fig. 7. Simulation results for the investigated cases at 90% load: (a) NO_x emissions, (b) CO emissions and (c) CO and in-cylinder temperature spatial distributions.

% MEF case. Fig. 7c presents the spatial distribution of CO emissions at crank angles of 1, 7 and 33°CA ATDC, which correspond to the end of diesel injection, the CA50 point, and after the combustion end, respectively. At the initial stages of combustion, CO is formed at regions of elevated in-cylinder temperature that are close to the fuel jet. For the PI, as shown at the plots corresponding to 1°CA ATDC, the high temperature region around the jet tail favours the CO accumulation close to the jet. Conversely at the same crank angle for the DI case, CO is formed within the jet region. Since the diffusive flame temperature is not high enough, the incomplete combustion favours CO formation. At 7°CA ATDC as premixed flame front propagates, the homogeneity of the air-methanol mixture allows for more uniform temperature distribution allowing uniform CO formation compared to the DI, where CO is concentrated at the low temperature flame front. By 33°CA ATDC, the combustion ends, and most the CO amount is converted to CO_2. For the DI case, the CO is concentrated close to the nozzle region and in the piston wall, where heat transfer interactions between wall and in-cylinder mixture reduce locally the temperature inhibiting the CO oxidation.

Fig. 8 illustrates the unregulated emissions of formaldehyde, which is considered a toxic substance even in small concentration. Formaldehyde is formed by the post-oxidation of unburned methanol. The derived results demonstrate that the formaldehyde concentration increases for higher MEF [61]. High in-cylinder temperature favours the methanol oxidation, and hence the formaldehyde concentration reduction. Cases with reduced charge temperature exhibited increased formaldehyde concentration. For DI cases with MEF above 50 %, high air–fuel ratio and charge temperature are responsible for the considerable decrease of the formaldehyde concentration. For DI cases with 20 % and 50 % MEF, high formaldehyde concentration is calculated, which is attributed to the heterogeneous mixture formation that inhibits methanol oxidation.

The formation of thermal NOx is favoured by high in-cylinder temperature, mixture homogeneity and ignition delay. Fig. 9 illustrates the relationship between thermal NOx formation, temperature increase, and methanol consumption for the 50 % MEF case for both PI (a) and DI (b) cases. Despite the higher mean in-cylinder temperature for PI, the residence time above the cut-off temperature is longer for DI, resulting in higher NOx concentration compared to PI. This extended residence time allows for more extensive chemical reactions at higher temperatures, primarily due to the longer combustion duration observed in the DI cases (as discussed in Section 3.1, Fig. 5). The increased area below the NOx curve before the cut-off point denotes higher NOx concentration. Therefore, combustion duration also greatly affects the NOx formation.

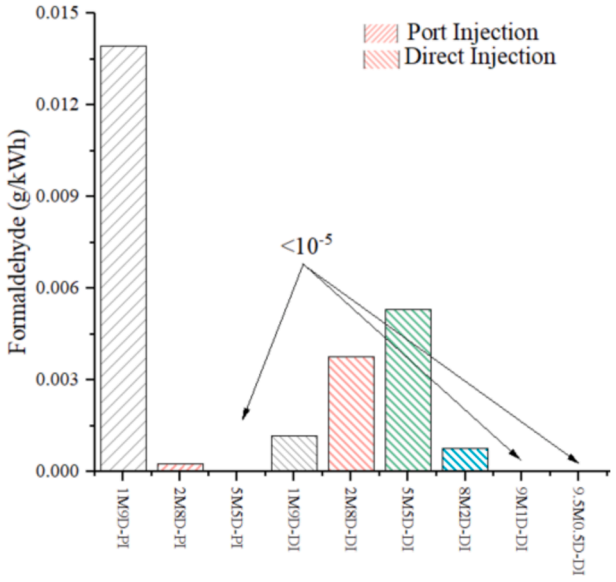

Fig. 8. Formaldehyde emissions for the considered cases.

Table 8 provides evidence to support the preceding remarks on the NOx emissions visually illustrating the NOx emissions contours for the PI and DI cases with 50 % MEF. The selected CA slices correspond to the initial combustion stages close to CA10 (1 and 3°CA ATDC), the intermediate stage close to CA50 and peak HRR (10°CA ATDC) and the stage towards the combustion end (27°CA ATDC). These two cases are selected for comparing the PI and DI cases, as 50 % MEF is the upper MEF boundary for the PI.

For the PI case, the methanol combustion flame front areas exhibit high temperature (above 2600 K), which triggers the NOx formation. As combustion progresses and methanol is consumed in the premixed flame front, local maxima of temperature close to 10°CA ATDC, lead to thermal NOx formation. Diesel diffusive combustion starts at around 1°CA ATDC. During the expansion phase, methanol is completely consumed while the temperature gradually decreases, although it remains sufficiently high (>1800 K) to facilitate the NOx radicals generation, a process that ceases after 27°CA ATDC.

For the DI case, the non-homogenous methanol–air mixture leads to higher temperatures at the diffusion combustion region compared to the PI case, resulting in higher NOx emissions. It is inferred from contour plots for 10°CA ATDC and 27°CA ATDC that the NOx concentration is greater for the DI case. For this case, the combustion ends at around 10°CA ATDC, leading to shorter combustion duration (compared to the PI), hence resulting in higher heat release rate, which, in turn, increases thermal efficiency and NOx emissions.

3.3. Engine parameters

Fig. 10 presents the indicated thermal efficiency for the investigated PI and DI cases. The former exhibit lower indicated efficiency for the same MEF with the difference increasing with MEF. For the PI cases, the indicated thermal efficiency reduced from 42 % in the BL case, to 41.7 %, 41.6 % and 41.4 % for cases with 10 %, 20 % and 50 % MEF respectively. This is attributed to the lower methanol LHV and therefore the increased fuel consumption. The DI cases yield higher indicated thermal efficiency to 42.5 %, 42.7 %, 44.1 %, 43.9 %, 43.8 % and 43.7 % for MEF 10 %, 20 %, 50 %, 80 %, 90 % and 95 %. This is attributed to the reduction in compression work as presented in Fig. C1 (Appendix C), that becomes more pronounced at higher MEF. The combustion substantially shortens at high MEF, further reducing the heat transfer losses, as discussed in [52].

Table 9 presents the percentage changes in several performance and emissions parameters for the investigated cases compared to the BL case (diesel mode). The parameters that considerably increase with MEF are the peak HRR, and the RI index. Contrary, smaller changes are exhibited in the peak in-cylinder temperature, which however, greatly affect the NO_x emissions. The peak in-cylinder temperature reduces with MEF, while the mean temperature at CA90 increases. This generates favourable conditions for NO_x formation, however, due to significantly lower combustion duration, the residence time at higher temperatures reduces, resulting in lower NO_x emissions. The trade-offs presented in Table 9 are in alignment with the pertinent literature findings [54,55].

For premixed combustion cases, the in-cylinder pressure and peak-HRR exhibited notable increase with MEF, attributed to the methanol higher oxygen content that shortens the combustion process. Homogenous methanol-air mixtures lead to increased ringing intensity that indicates knocking. As knocking constrains the use of high MEFs, methanol-diesel dual fuel engines operations above 50 % MEF are plausible only for direct injection cases. Direct injection marine engines exhibit higher indicated thermal efficiency as well as lower NOx and CO emissions compared to diesel. For considerably reducing NOx and CO emissions in marine engines, premixed combustion with up to 50 % MEF is proposed. Such methanol–diesel dual fuel engine is expected to present lower indicated thermal efficiency than diesel operation.

This study relies on CFD simulations, which are inherently dependent on several assumptions pertinent to boundary conditions, whereas

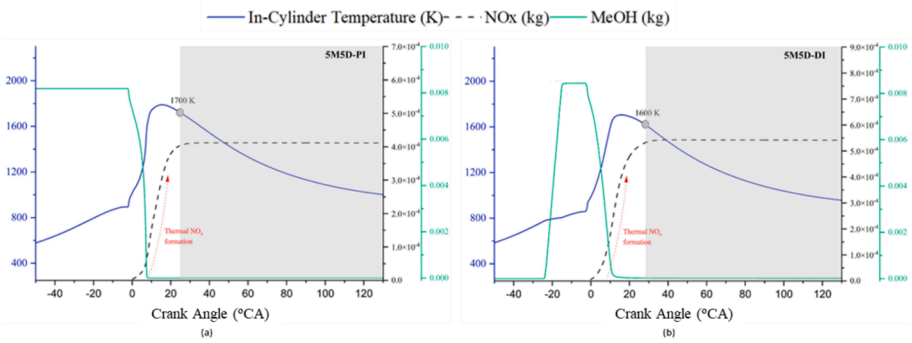

Fig. 9. NO_x emissions variation for 50% MEF at 90% load: (a) 5M5D-PI case, and (b) 5M5D-DI case.

Table 8
CFD results for the 5M5D-PI (a) and 5M5D-DI (b) cases at 90% load.

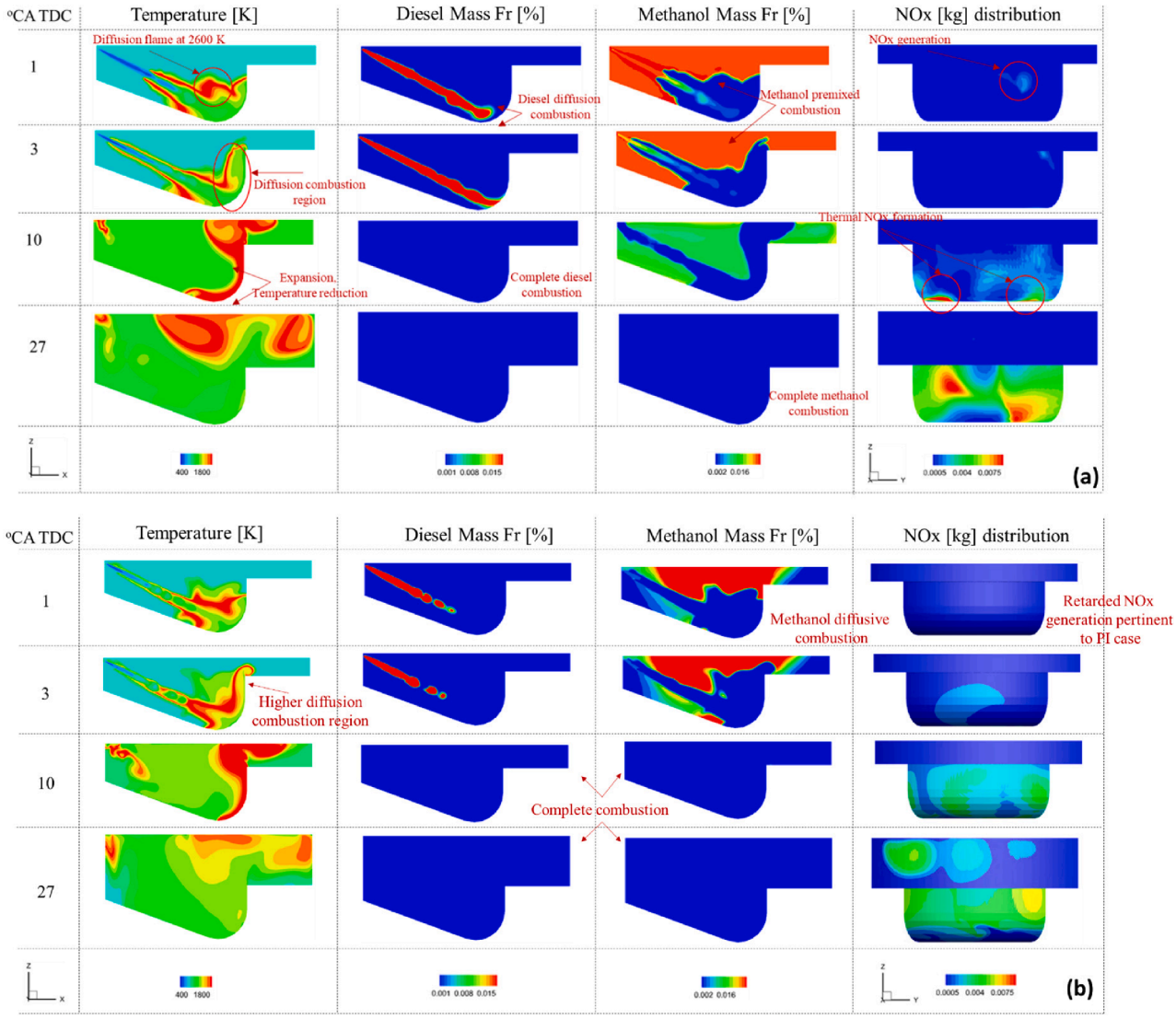

chemical kinetics may introduce uncertainties in the results accuracy. While CFD simulations provide useful trade-offs of the engine performance and emissions parameters, the lack of comprehensive experimental validation in real-world engine conditions is a limitation of this study. The study focusses on a specific range of operating conditions or a particular engine configuration. Extending the findings to a broader range of conditions or different engine types may be challenging, requiring future studies. This comparative assessment led to the identification of significant challenges and advantages associated with the considered methanol injection methods and MEF, hence contributing to a better understanding of the key optimisation requirements for the investigated engine.

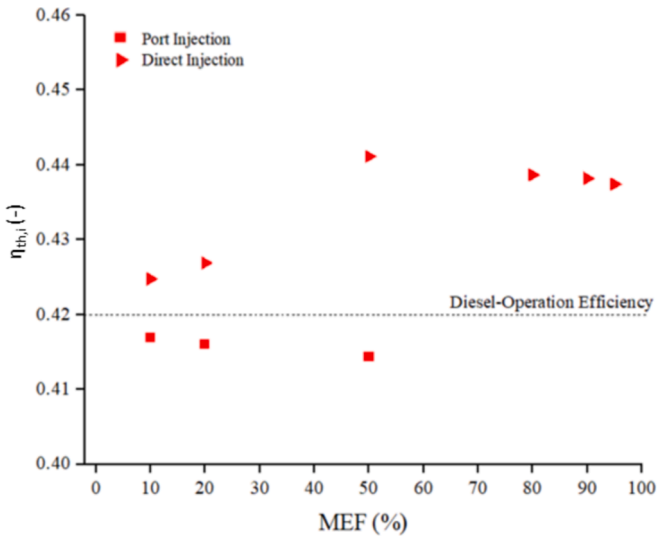

Fig. 10. Effect of MEF on indicated thermal efficiency.

3.4. Comparison of large and small-bore engines

This section qualitatively examines the variations of several parameters (maximum in-cylinder pressure and temperature, NOx emissions, and indicated thermal efficiency) for small-bore engines using methanol, based on a previous authors' study [56] reporting the impact of MEFs on these parameters. For the premixed combustion engines with nominal power output between 4 kW and 220 kW, MEF increase leads to longer ignition delays and higher heat release rate peaks, hence exhibiting similar trade-offs with the investigated marine engine herein. The maximum MEF for these engines for achieving knock-free combustion was reported to be 47–50 %, which aligns with the 50 % MEF limit identified for the investigated marine engine.

For direct injection methanol engines with nominal power between 8 kW and 2.3 MW, MEF ranging 5–40 % results in brake efficiency reduction by 2–10 %., whereas similar MEF values led to brake efficiency increase by 1–5 % for the investigated marine engine herein. Most of the studies reported reduction of NOx emissions compared to the diesel mode, which is in alignment with this study findings. Low MEF values (5–8 %) resulted in considerable NOx emissions increase, which also aligns with the 8 % NOx emissions increase found herein for the investigated marine engine operating with 10 % MEF. The studies considered in Ref [56] considered MEFs between 5 % and 40 % for the DI engines, whereas trade-offs for engine operating with higher MEF values are not reported in the literature.

It is worth noting that the injection settings and initial conditions may also influence the engine performance and emissions parameters. Hence, it is recommended future studies deal with comprehensive scaling analysis and validating this study results against experimental data.

4. Conclusions

This study conducted a parametric investigation to determine the impact of methanol energy fraction (MEF) in a dual-fuel marine engine considering premixed combustion (with methanol port injection) and methanol direct in-cylinder injection. CFD models were developed for these modes and the diesel mode. These CFD models were validated against experimental data for the investigated engine operating in the diesel mode and gas mode, whereas validation against reported experimental results for a small methanol fuelled engine was also performed. The study concluded in the following findings:

- For premixed combustion, increased in-cylinder pressure and unstable combustion were exhibited with MEF, limiting the upper MEF to 50 %.
- Port methanol injection at 50 % MEF present significant benefits for the considered marine engine, reducing NOx emissions by 30.5 % compared to the diesel mode.
- For premixed combustion, the marine engine exhibited lower thermal efficiency compared to its diesel mode (41.6 % for 50 % MEF compared to 42 % for diesel).
- Premixed combustion method is preferred for retrofitting existing engines as fewer modifications are required in the engine head and manifolds.
- Direct methanol injection demonstrates knock-free combustion (RI within the acceptable limits) up to 95 % MEF, and hence it is preferred when higher decarbonisation levels are required.
- For direct methanol injection, the NOx and CO emissions are lower compared to the diesel mode, whereas thermal efficiency increases by 1–4.2 % for MEF 10–95 %. The latter is attributed to faster combustion, reduction of compression work and heat losses reduction for high MEF.
- The use of methanol direct injection with high MEF in dual-fuel marine engines proved to be feasible as knock-free combustion conditions can be achieved. However, for low MEF, the use of the premixed combustion proved advantageous, as it considerably reduces NOx and CO emissions.

This study provided insights for the marine dual-fuel engines operating with methanol, and hence contributes towards the development of sustainable shipping. This study limitations are associated to the experimental validation of the dual-fuel diesel-methanol cases. Future studies could consider the optimisation of the engine systems settings, configurations (injection, turbocharger, EGR, etc.) and injection strategies to achieve knock-free conditions with improved engine performance and reduced emissions.

CRediT authorship contribution statement

Panagiotis Karvounis: Writing – original draft, Methodology, Conceptualization. **Gerasimos Theotokatos:** Writing – review & editing, Supervision, Project administration. **Chaitanya Patil:** Writing –

Table 9
MEF effect on the derived parameters compared to the baseline case.

Case	Parameter percentage change (%)								
	p_{max}	T_{max}	T_{mean} at CA90	HRR_{peak}	CA50	CA90	NO_x	RI	η_c
1M9D-PI	+1.6	−1.3	−1	+5	−4.11	+1.62	−22.03	−7	−0.64
2M8D-PI	+8.1	−2	+3	+23	−19.18	−0.65	−25.42	+44	−0.85
5M5D-PI	+33.9	−3	+5	+318	−52.05	−70	−30.51	+62	−1.24
1M9D-DI	+5.9	−2	+2	+5	−13.01	−10.06	+7.97	+7	1.24
2M8D-DI	+9.9	−2	+1	+13	−19.86	−10.06	−1.19	+21	1.74
5M5D-DI	+29.8	−3	+4	+225	−50.68	−43.51	−8.47	+62	5.14
8M2D-DI	+53.7	−9	+9	+458	−93.15	−79.87	−71.19	+74	4.55
9M1D-DI	+51.4	−3	+13	+437	−85.62	−84.74	−50.85	+78	4.44
9.5 M0.5D-DI	+37.8	−3.5	+13	+293	−48.63	−67.21	−85.17	+79	4.26

review & editing, Software, Methodology, Data curation. **La Xiang:** Software, Methodology. **Yu Ding:** Writing – review & editing, Supervision.

Declaration of competing interest

The authors declare that they have no known competing financial interests or personal relationships that could have appeared to influence the work reported in this paper.

Acknowledgments

Part of this study was carried out in the framework of the project "Highly Efficient Retrofitted Zero Emissions Coaster (HEROZEC)" (No. 10098828), which were funded by the Innovate UK. The authors greatly acknowledge the funding from DNV AS and RCCL for the MSRC establishment and operation. The opinions expressed herein are those of the authors and should not be construed to reflect the views of DNV AS and RCCL. The opinions expressed herein are those of the authorsand should not be construed to reflect the views of Innovate UK, DNV AS, RCCL, and the HEROZEC partners.

Appendix A. : Diesel and methanol grid sensitivity study

The CFD model employs an intrinsic mesh control strategy that includes a base grid size along with adaptive mesh refinement. The performed grid sensitivity study determines the computational grid impact on the model accuracy, while simultaneously considering the required computational effort. The employed grids, listed in Table 4, consist of elements with sizes of 12, 10,8 and 6 mm, which are deemed suitable for the investigated marine engine cylinder size. Fig. A1a presents the spatial distribution of NOx emissions and maximum in-cylinder temperature, whereas Fig. A1(b and c) presents the mean temperature and pressure in-cylinder variations.

The root mean square error considered the simulated and measured in-cylinder pressure is calculated according to the following equation and employed for assessing the model results accuracy:

$$RMSE = \sqrt{\left(\frac{\sum_{i=1}^{n}(y_i - \hat{y}_i)^2}{n}\right)} \tag{5}$$

where, n refers to the number of collected data, y_i and $\hat{y}_i$ correspond to measured and calculated values of in-cylinder pressure, respectively.

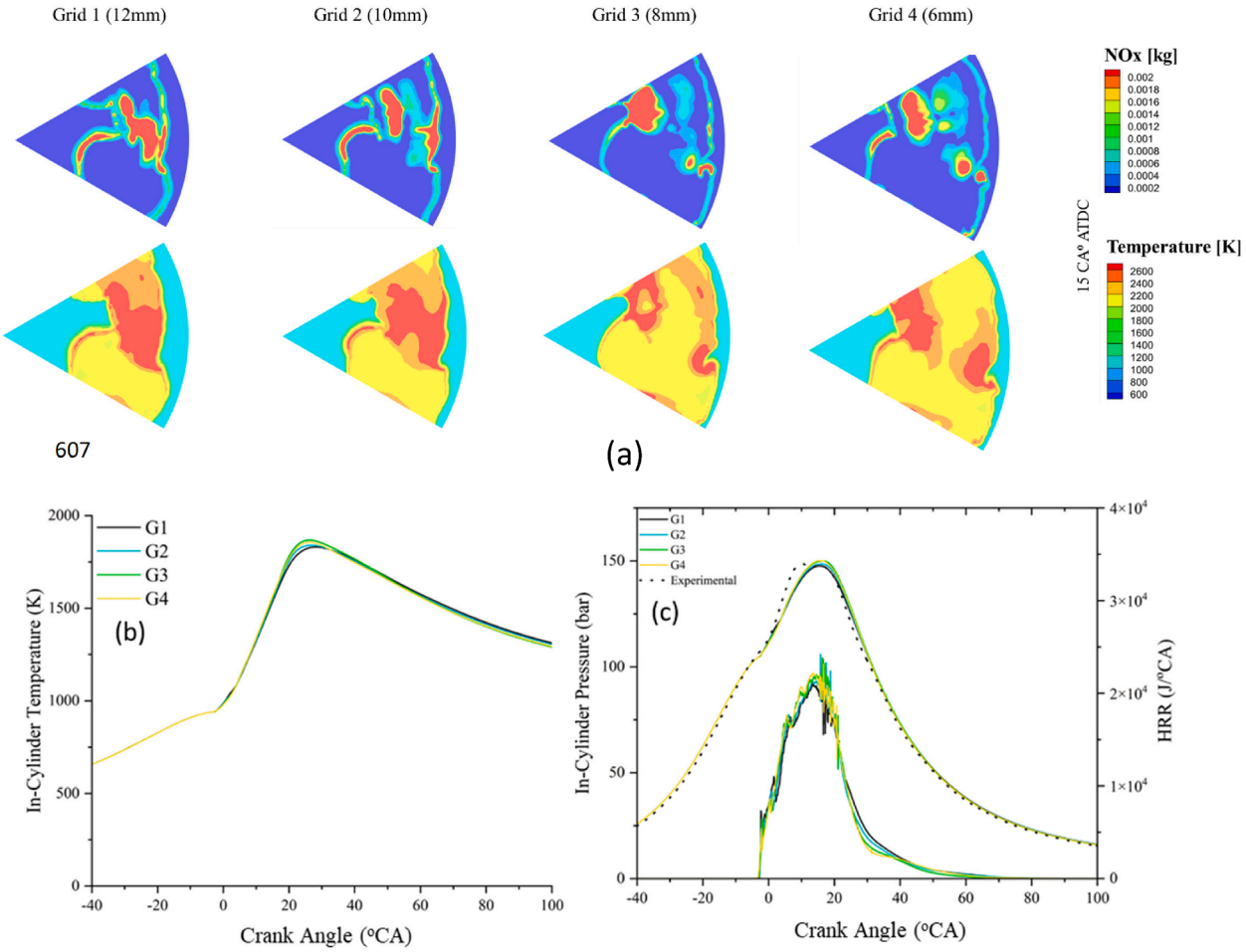

Fig. A1. Grid sensitivity study results for the diesel mode at 50 % load: (a) spatial variations of NOx concentration and in-cylinder temperature for several crank angles; (b) mean in-cylinder temperature, and; (c) mean in-cylinder pressure and heat release rate.

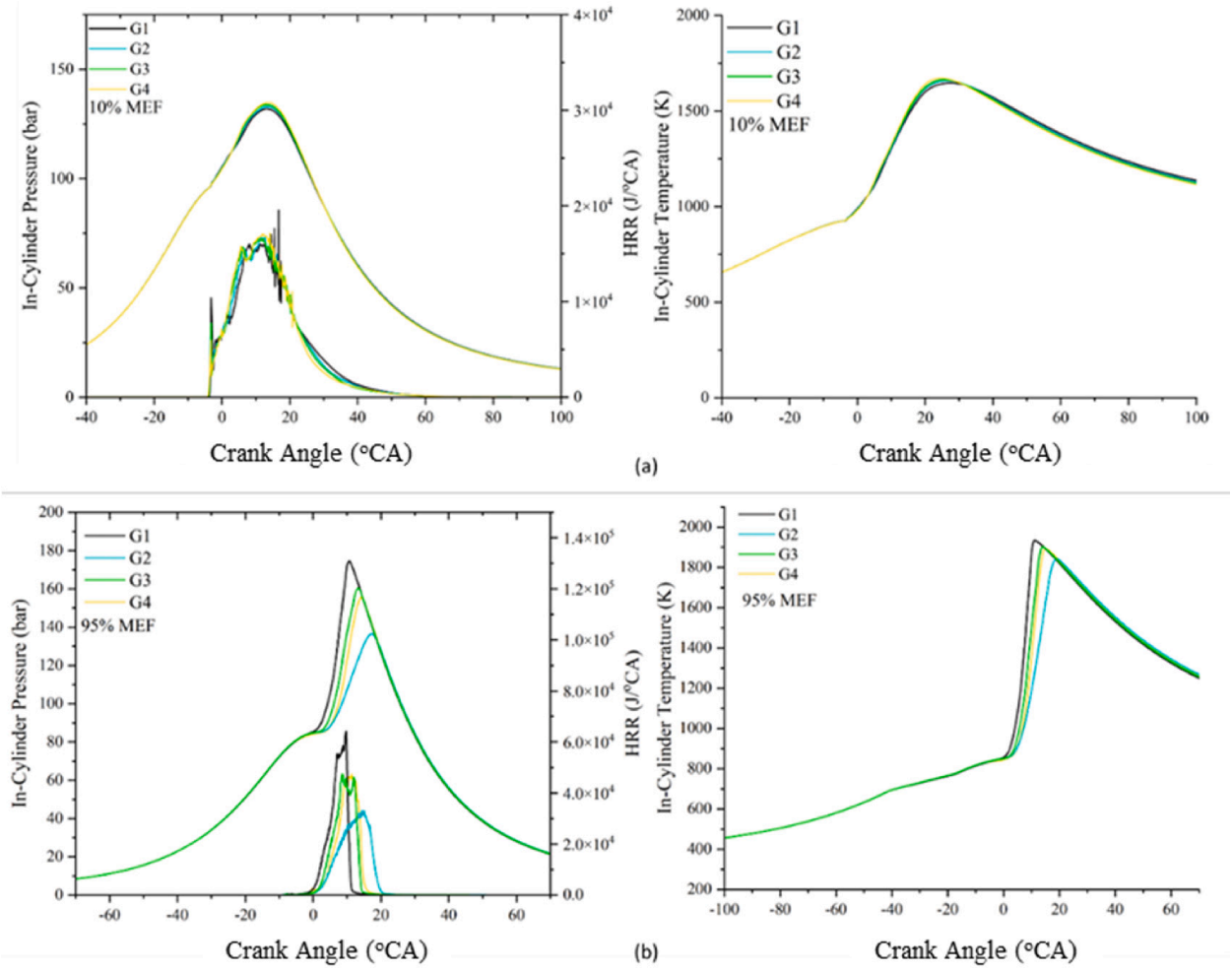

Fig. A2. Grid sensitivity results – in-cylinder pressure, heat release rate and mean temperature for: (a) 10 % MEF-PI, and; (b) 95 % MEF-DI.

Table A1 includes the grids particulars and the computational time of the developed CFD model. The variation of in-cylinder pressure, heat release rate and in-cylinder temperature for the cases 1M9D-PI and 9.5 M0.5D-DI are presented in Fig. A2. Grid 3 exhibits a compromise between accuracy and computational effort, hence it was selected for the simulation runs conducted for the methanol PI/DI cases.

Table A1
Methanol grid characteristics.

Parameter	Grid 1	Grid 2	Grid 3	Grid 4
Element size (mm)	12	10	8	6
Maximum Number of Cells*	10,900	18,838	36,800	87,216
Adaptive mesh refinement	On	On	On	On
Simulation run duration (h)	4	5.5	11	46

Appendix B:. Injection parameters

Table B1 lists the injection parameters provided as input to the developed CFD models for the investigated cases. Injection pressure is kept constant for all cases. Additionally, the injector orientation is not considered herein. Methanol and diesel are injected from different nozzles of the same injector. Methanol nozzles have the same geometrical characteristics with the diesel nozzles.

Table B1
Injection parameters.

Methanol Injection Method	Case Study Code	Diesel Injection Duration (°CA)	Methanol Injection Duration (°CA)	Mass of Diesel Injected (mg)	Mass of Methanol Injected (mg)	Methanol/Diesel Injection Pressure (bar)
	BL	22	–	1300	–	– / 1000
Port Injection	1M9D-PI	20	port	1200	300	1400/1000
	2M8D-PI	18	port	1100	600	
	5M5D-PI	11	port	700	1400	
	6MD4-PI	8	Port	555	1760	
	8M2D-PI	6	port	300	2200	
Direct Injection	1M9D-DI	21	11	1200	300	
	2M8D-DI	20	11	1100	600	
	5M5D-DI	12	11	700	1400	
	8M2D-DI	5	30	300	2200	
	9M1D-DI	5	30	140	2500	
	9.5 M0.5D-DI	5	30	70	2800	

Appendix C:. Compression work reduction

Fig. C1 illustrates the pressure diagram area corresponding to the compression work reduction comparing the baseline (diesel mode) case and the DI case with 95 % MEF.

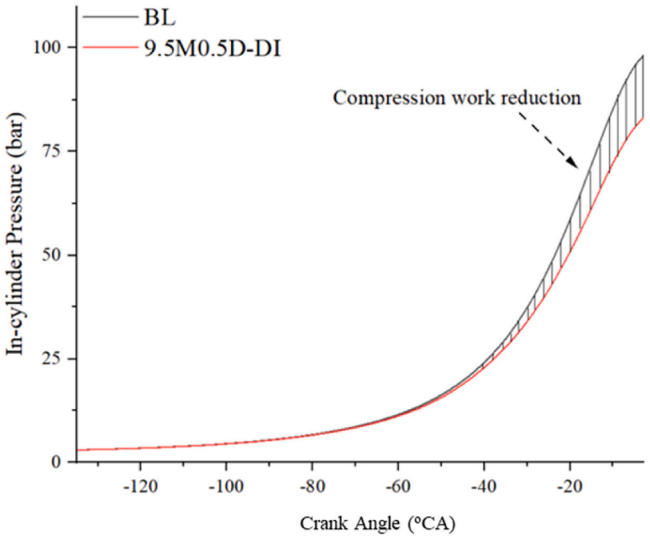

Fig. C1. Pressure diagrams and area denoting the compression work reduction between the baseline case and DI case with 95 % MEF.

Appendix D:. Contour plots for in-cylinder pressure and oxygen concentration

Fig. D1 presents the in-cylinder pressure and the oxygen concentration close to TDC before the start of combustion, which are employed to define the mixture reactivity (the ability of substances to react under specific in-cylinder conditions) for 50 % MEF PI and DI cases.

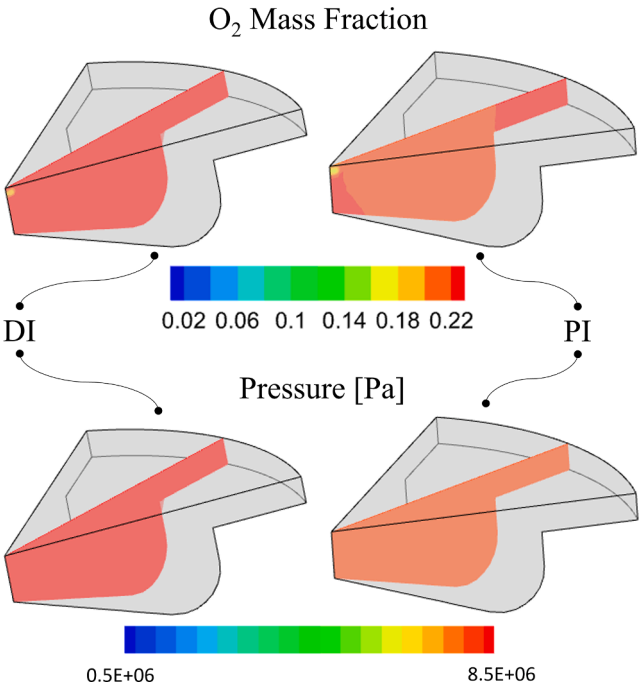

Fig. D1. In-cylinder pressure and oxygen concentration at 5°CA BTDC for 50 % MEF PI and DI cases.

Appendix E:. CFD model results for the investigated marine engine operating in the gas mode

The developed CFD model was employed to simulate the closed cycle of the investigated marine engine operation in the gas mode. The engine operates based on the premixed combustion concept; the natural gas is in injected in the engine cylinders ports, whereas pilot diesel is directly injected within the engine cylinders to initiate the natural gas combustion. The available experimental data were measured during the engine shop test trials. Table E1 lists the simulated and measured indicated power, maximum in-cylinder pressure, and NOx emissions for four different loads (25 %, 50 %, 75 % and 100 %).

Table E1
Simulated and measured (shop tests) indicated power, maximum in-cylinder pressure, and NOx emissions for the considered marine engine operation in the gas mode.

Load (%)	Indicated power			Maximum cylinder pressure			NOx emissions		
	Measured (kW)	Simulation (kW)	Error (%)	Measured (bar)	Simulation (bar)	Error (%)	Measured (g/kWh)	Simulation (g/kWh)	Error (%)
25	1950	1900	3.6	38	38	0	9.15	9.9	8.6
50	3900	3950	2.3	64	66	4.1	9.7	10.1	4
75	5850	5700	3.6	92	90	3.2	9.7	10.4	7.8
100	7800	7890	2.2	126	125	1.8	9.43	10	6.7

Data availability

No data was used for the research described in the article.

References

[1] Falkner R. The Paris Agreement and the new logic of international climate politics. Int Aff 2016;92(5):1107–25.
[2] Chen L, Yip TL, Mou J. Provision of Emission Control Area and the impact on shipping route choice and ship emissions. Transp Res Part D: Transp Environ 2018; 58(280–291):2018.
[3] Polakis M, Zachariadis P, Kat JOD. The energy efficiency design index (EEDI). In: Sustainable shipping. Springer; 2019. p. 93–135.
[4] Lindstad, E., Dražen, P., Rialland, A., Sandaas, I., & Stokke, T. Reaching IMO 2050 GHG Targets Exclusively through Energy efficiency measures. In SNAME Maritime Convention, 2022.
[5] McKinlay CJ, Turnock SR, Hudson DA. Route to zero emission shipping: Hydrogen, ammonia or methanol? Int J Hydrogen Energy 2021;46(55):28282–97.
[6] Svanberg M, Ellis J, Lundgren J, Landälv I. Renewable methanol as a fuel for the shipping industry. Renew Sustain Energy Rev 2018;94:1217–28.
[7] Public Final Report MIIP001-2017..
[8] Karvounis, P., Tsoumpris, C., Boulougouris, E., Theotokatos, G. Recent advances in sustainable and safe marine engine operation with alternative fuels. Frontiers in Mechanical Engineering, 8, 994942, doi: 10.3389/fmech.2022.994942.
[9] Datta A, Mandal BK. Impact of alcohol addition to diesel on the performance of combustion and emissions of a compression ignition engine. Appl Therm Eng 2016; 98:670–82.
[10] Chinmaya M, Anuj P, Singh TV, Naveen K. Combustion, Emission and Performance Characteristics of a Light Duty Diesel Engine Fueled with Methanol Diesel Blends. International Scholarly and Scientific Research & Innovation 2013;7(5).
[11] Ning L, Duan Q, Chen Z, Kou H, Liu B, Yang B, et al. A comparative study on the combustion and emissions of a non-road common rail diesel engine fueled with primary alcohol fuels (methanol, ethanol, and n-butanol)/diesel dual fuel. Fuel 2020;266:117034. https://doi.org/10.1016/j.fuel.2021.121360.
[12] Li Y, Jia M, Liu Y, Xie M. Numerical study on the combustion and emission characteristics of a methanol/diesel reactivity controlled compression ignition (RCCI) engine. Appl Energy 2013;106:184–97. https://doi.org/10.1016/j.apenergy.2013.01.058.
[13] Wei L, Yao C, Han G, Pan W. Effects of methanol to diesel ratio and diesel injection timing on combustion, performance and emissions of a methanol port premixed

diesel engine. Energy 2016;95:223–32. https://doi.org/10.1016/j.energy.2015.12.020.
[14] Li Z, Wang Y, Yin Z, Gao Z, Wang Y, Zhen X. To achieve high methanol substitution ratio and clean combustion on a diesel/methanol dual fuel engine: A comparison of diesel methanol compound combustion (DMCC) and direct dual fuel stratification (DDFS) strategies. Fuel 2021;304:121466.
[15] Li Z, Wang Y, Geng H, Zhen X, Liu M, Xu S, et al. Parametric study of a diesel engine fueled with directly injected methanol and pilot diesel. Fuel 2019;256:115882.
[16] Valentino G, Corcione FE, Iannuzzi SE, Serra S. Experimental study on performance and emissions of a high speed diesel engine fuelled with n-butanol diesel blends under premixed low temperature combustion. Fuel 2012;92(1):295–307.
[17] Wang Q, Wei L, Pan W, Yao C. Investigation of operating range in a methanol fumigated diesel engine. Fuel 2015;140:164–70.
[18] Liu J, Li G, Zhu Z, He H, Liu S. Effect of pilot diesel quantity and fuel delivery advanced angle on the performance and emissions characteristics of a methanol fueled diesel engine. Energy Fuel 2010;24:1611–6.
[19] Song R, Liu J, Wang L, Liu S. Performance and emissions of a diesel engine fuelled with methanol. Energy Fuel 2008;22:3883–8.
[20] Coulier J, Verhelst S. Using Alcohol Fuels in Dual Fuel Operation of Compression Ignition Engines: A Review. Helsinki: CIMAC Congress; 2016.
[21] Dierickx, J., Sileghem, L., & Verhelst, S. (2019). Efficiency and emissions of a high-speed marine diesel engine converted to dual-fuel operation with methanol. In CIMAC World Congress on Combustion Engine (pp. 1-14). CIMAC.
[22] The methanol fuelled MAN B&W LGIM engine, MAN Energy Solutions, Application, service experience and latest development of the ME-LGIM engine. Available at: https://www.man-es.com/docs/default-source/document-sync/the-methanol-fuelled-man-b-w-lgim-engine63e54a8470694265bdeb07314c4f0e11.pdf?sfvrsn=148c08f0_0.
[23] WÄRTSILÄ 32 Methanol, Product Guide, Available at: https://www.wartsila.com/marine/products/engines-and-generating-sets/wartsila-32-methanol-engine.
[24] MAN L21/31DF-M methanol GenSet, Product Guide, Available at: https://www.man-es.com/marine/campaigns/man-l21-31df-m.
[25] Bahri B, Shahbakhti M, Kannan K, Aziz AA. Identification of ringing operation for low temperature combustion engines. Appl Energy 2016 Jun;1(171):142–52.
[26] Stoumpos S, Theotokatos G, Boulougouris E, Vassalos D, Lazakis I, Livanos G. Marine dual fuel engine modelling and parametric investigation of engine settings effect on performance-emissions trade-offs. Ocean Eng 2018;157:376–86.
[27] Ricart LM, Reitz RD, Dec JE. Comparisons of diesel spray liquid penetration and vapor fuel distributions with in-cylinder optical measurements. J Eng Gas Turb Power 2000;122(4):588–95.
[28] Han ZY, Xu Z, Trigui N. Spray/wall interaction models for multidimensional engine simulation. Int J Eng Res 2000;1(1):127–46.
[29] Schmidt DP, Rutland CJ. A New Droplet Collision Algorithm. J Comput Phys 2000;164(1):62–80. https://doi.org/10.1006/jcph.2000.6568.
[30] Han ZY, Reitz RD. A temperature wall function formulation for variable density turbulence flows with application to engines convective heat transfer modeling. Int J Heat Mass Transfer 1997;40(3):613–25.
[31] Zeldovich YB. The Oxidation of Nitrogen in Combustion Explosions. Acta Physicochimica USSR 1946;21:577–628.
[32] Zhang C, Wu H. Combustion characteristics and performance of a methanol fueled homogenous charge compression ignition (HCCI) engine. J Energy Inst 2016 Aug 1;89(3):346–53.
[33] Andrae JC, Head RA. HCCI experiments with gasoline surrogate fuels modeled by a semidetailed chemical kinetic model. Combust Flame 2009 Apr 1;156(4):842–51.
[34] Tsitsilonis KM, Theotokatos G, Patil C, Coraddu A. Health assessment framework of marine engines enabled by digital twins. Int J Engine Res 2023;12.14680874221146835.
[35] Siebers DL. Liquid-phase fuel penetration in diesel sprays. SAE Trans 1998;1:1205–27.
[36] Dernotte J, Dec J, Ji C. Investigation of the sources of combustion noise in HCCI engines. SAE Int J Engines 2014;7(2):730–61.
[37] MAN Diesel & Turbo SE, "Technical paper: Pressure rise rates in medium-speed diesel engines," 2012.
[38] Kokkulunk G, Parlak A, Erdem HH. Determination of performance degradation of a marine diesel engine by using a curve-based approach. Appl Therm Eng 2016;108:1136. https://doi.org/10.1016/j.applthermaleng.2016.08.019.
[39] Wang R, Chen H, Guan C. A Bayesian inference-based approach for performance prognostics towards uncertainty quantification and its applications on the marine diesel engine. ISA Trans 2021;118:159–73. https://doi.org/10.1016/j.isatra.2021.02.024.
[40] Yin X, Xu L, Duan H, Wang Y, Wang X, Zeng K, et al. In-depth comparison of methanol port and direct injection strategies in a methanol/diesel dual fuel engine. Fuel Process Technol 2023;241:107607.
[41] Yin X, Li W, Zhang W, Lv X, Yang B, Wang Y, et al. Experimental analysis of the EGR rate and temperature impact on combustion and emissions characteristics in a heavy-duty NG engine. Fuel 2022;310:122394.
[42] Senecal P, Pomraning E, Richards K, Briggs T, et al. Multi-Dimensional Modeling of Direct-Injection Diesel Spray Liquid Length and Flame Lift-off Length using CFD and Parallel Detailed Chemistry. SAE Technical Paper 2003–01-1043, 2003,. https://doi.org/10.4271/2003-01-1043.
[43] Duan Q, Yin X, Wang X, Kou H, Zeng K. Experimental study of knock combustion and direct injection on knock suppression in a high compression ratio methanol engine. Fuel 2022;311:122505.
[44] Lounici MS, Benbellil MA, Loubar K, Niculescu DC, Tazerout M. Knock characterization and development of a new knock indicator for dual-fuel engines. Energy 2017;141:2351–61.
[45] Tutak W, Lukács K, Szwaja S, Bereczky Á. Alcohol–diesel fuel combustion in the compression ignition engine. Fuel 2015;154:196–206.
[46] Dierickx J, Mattheeuws L, Christianen K, Stenzel K, Verhelst S. Evaluation and extension of ignition delay correlations for dual-fuel operation with hydrogen or methanol in a medium speed single cylinder engine. Fuel 2023;345:128254.
[47] Saxena MR, Maurya RK, Mishra P. Assessment of Performance, Combustion and Emissions Characteristics of Methanol-Diesel Dual-Fuel Compression Ignition Engine: A Review. J Traffic Transp Eng 2021;8(5):638–80. https://doi.org/10.1016/j.jtte.2021.02.003.
[48] Wang B, Yao A, Yao C, Chen C, Wang H. In-Depth Comparison between Pure Diesel and Diesel Methanol Dual Fuel Combustion Mode. Appl Energy 2020;278:115664. https://doi.org/10.1016/j.apenergy.2020.115664.
[49] Y. Cui Z. Zheng M. Wen Q. Tang C., Geng, Q., Wang, Liu, H., Yao, M., Optical diagnostics on the effects of reverse reactivity stratification on the flame development in dual-fuel combustion 2021.
[50] Dierickx J, Verbiest J, Janvier T, Peeters J, Sileghem L, Verhelst S. Retrofitting a high-speed marine engine to dual-fuel methanol-diesel operation: A comparison of multiple and single point methanol port injection. Fuel Communications 2021;7:100010.
[51] Saccullo M, Benham T, Denbratt I. Dual fuel methanol and diesel direct injection HD single cylinder engine tests. SAE Technical Paper Series 2018.
[52] 53. Chinmaya M, Anuj P, Singh TV, Naveen K. Combustion, Emission and Performance Characteristics of a Light Duty Diesel Engine Fueled with Methanol Diesel Blends. Int Scholarly Sci Res Innov 2013;7(5).
[54] Zhen X, Wang Y. An overview of methanol as an internal combustion engine fuel. Renew Sustain Energy Rev 2015;52:477–93.
[55] Verhelst S, Turner JWG, Sileghem L, Vancoillie J. Methanol as a fuel for internal combustion engines. Prog Energy Combust Sci 2019;70:43–88.
[56] Karvounis P, Theotokatos G, Vlaskos I, Hatziapostolou A. Methanol combustion characteristics in compression ignition engines: a critical review. Energies 2023 Dec 14;16(24):8069.
[57] Zang R, Yao C. Numerical study of combustion and emission characteristics of a diesel/methanol dual fuel (DMDF) engine. Energy Fuel 2015 Jun 18;29(6):3963–71.
[58] Li J, Wang J, Liu T, Dong J, Liu B, Wu C, et al. An investigation of the influence of gas injection rate shape on high-pressure direct-injection natural gas marine engines. Energies 2019 Jul 4;12(13):2571.
[59] Xu C, Zhuang Y, Qian Y, Cho H. Effect on the performance and emissions of methanol/diesel dual-fuel engine with different methanol injection positions. Fuel 2022 Jan;1(307):121868.
[60] Bravo L, Kweon CB. A review on liquid spray models for diesel engine computational analysis. Army Research Laboratory Technical Report Series, ARL-TR-6932. 2014 May 1.
[61] Zhang Y, Mu Z, Wei Y, Zhu Z, Du R, Liu S. Comprehensive study on unregulated emissions of heavy-duty SI pure methanol engine with EGR. Fuel 2022;320:123974.
[62] Shi M, Wu B, Wang J, Jin S, Chen T. Optimization of methanol/diesel dual-fuel engines at low load condition for heavy-duty vehicles to operated at high substitution ratio by using single-hole injector for direct injection of methanol. Appl Therm Eng 2024 Jun;1(246):122854.
[63] Amsden AA, O'Rourke PJ, Butler TD, "kiva-ii,. A Computer Program for Chemically Reactive Flows with Sprays,". Los Alamos National Laboratory Technical Report LA-11560-MS 1989.